Theoretical Framework for Measuring Cloud Effective Supersaturation Fluctuations with an Advanced Optical System

Ye Kuang[1], Jiangchuan Tao[1], Hanbin Xu[2], Li Liu[3], Pengfei Liu[4], Wanyun Xu[5], Weiqi Xu[6], Yele Sun[6], Chunsheng Zhao[7]

[1] Institute for Environmental and Climate Research, College of Environment and Climate, Jinan University, Guangzhou, Guangdong, China

[2] Experimental Teaching Center, Sun Yat-Sen University, Guangzhou, China

[3] Key Laboratory of Regional Numerical Weather Prediction, Institute of Tropical and Marine Meteorology, China Meteorological Administration, Guangzhou, China.

[4] School of Earth and Atmospheric Sciences, Georgia Institute of Technology, Atlanta, GA, USA

[5] State Key Laboratory of Severe Weather, Key Laboratory for Atmospheric Chemistry, Institute of Atmospheric Composition, Chinese Academy of Meteorological Sciences, Beijing, China

[6] State Key Laboratory of Atmospheric Boundary Layer Physics and Atmospheric Chemistry, Institute of Atmospheric Physics, Chinese Academy of Sciences, Beijing, China.

[7] Department of Atmospheric and Oceanic Sciences, School of Physics, Peking University, Beijing, China.

Correspondence: Ye Kuang (kuangye@jnu.edu.cn)

Abstract

Supersaturation is crucial in cloud physics, determining aerosol activation and influencing cloud droplet size distributions, yet its measurement remains challenging and poorly constrained. This study proposes a theoretical framework to simultaneously observe critical activation diameter and hygroscopicity of activated aerosols through direct measurements of scattering and water induced scattering enhancement of interstitial and activated aerosols, enabling effective supersaturation measurements. Advanced optical systems based on this framework allows minute- to second-level effective supersaturation measurements, capturing fluctuations vital to cloud microphysics. Although currently limited to clouds with supersaturations below ~0.2% due to small scattering signals from sub-100 nm aerosols, advancements in optical sensors could extend its applicability. Its suitability for long-term measurements allows for climatological studies of fogs and mountain clouds. When equipped with aerial vehicles, the system could also measure aloft clouds. Therefore, the proposed theory serving a valuable way for both short-term and long-term cloud microphysics and aerosol-cloud interaction studies.

1. Introduction

Clouds and fogs play critical roles in weather patterns and climate change, influencing both precipitation and the radiative balance of the Earth's atmosphere. As such, they are central to accurate weather and climate predictions. ~~Despite their importance, representing clouds accurately in atmospheric models remains a significant challenge (Seinfeld et al., 2016).~~Despite their importance, representing clouds accurately in atmospheric models remains a significant challenge (Seinfeld and Pandis, 2016) . Supersaturation, defined as the difference between the actual water vapor pressure (e) and the saturation vapor pressure (es) which is typically expressed as a dimensionless quantity (e−es)/es, is a key parameter that links aerosols to clouds through the process of aerosol activation, making it fundamental to cloud physics (Seinfeld and Pandis, 2016). Despite its importance, supersaturation is difficult to measure and remains poorly understood and constrained (Yang et al., 2019). Previous studies have highlighted that other than the mean supersaturation, supersaturation fluctuations also play critical roles in aerosol activation and cloud droplet growth, ultimately influencing the evolution of cloud droplet size distributions (Kaufman and Tanré, 1994;Sardina et al., 2015;Chandrakar et al., 2018;Chandrakar et al., 2020;Shaw et al., 2020). For instance, cloud chamber experiments have shown that supersaturation fluctuations promote aerosol activation and enhance aerosol activity (Shawon et al., 2021;Anderson et al., 2023), particularly when the magnitude of these fluctuations is comparable to the mean supersaturation (Prabhakaran et al., 2020). Both experimental and theoretical analyses suggest that supersaturation fluctuations can broaden cloud droplet size distributions (Chandrakar et al., 2016;Abade et al., 2018;Saito et al., 2019).

Supersaturation fluctuations arise not only from turbulent variations in the temperature and vapor pressure fields but also from the growth and evaporation of droplets, which drive mass and heat exchange between droplets and the surrounding air. ~~Field measurements have demonstrated that the supersaturation is indeed a fluctuating quantity (Ditas et al., 2012;Siebert and Shaw, 2017). However, as~~As noted by Shaw et al. (2020), measuring supersaturation remains a formidable challenge due to its extreme sensitivity to variations in ~~e and temperature.~~water vapor pressure and temperature. Although current techniques of water vapor and temperature measurements could not achieve accurately measurements of supersaturation, however, direct measurements of water vapor pressure and temperature were previously used to estimate supersaturation fluctuations, and obtained results have demonstrated that the supersaturation is indeed a fluctuating quantity (Ditas et al., 2012;Siebert and Shaw, 2017).. Currently, cloud and fog supersaturation are typically retrieved from aerosol activation measurements (Ditas et al., 2012) or estimated from vertical velocity measurements ~~(Siebert~~

and Shaw, 2017). Direct measurements of water vapor pressure and temperature are generally used to estimate supersaturation fluctuations but do not provide precise direct supersaturation measurements (Ditas et al., 2012;Siebert and Shaw, 2017).and droplet size distribution measurements (Siebert and Shaw, 2017;Cooper, 1989). Supersaturation parameterizations based on vertical velocity are common in models (Abdul-Razzak et al., 1998), while field measurements often rely on aerosol activation data to investigate supersaturation fluctuations and evolutions in clouds and fogs (Ditas et al., 2012;Hammer et al., 2014;Shen et al., 2018;Mazoyer et al., 2019;Zíková et al., 2020;Wainwright et al., 2021;Kuang et al., 2024). In addition, supersaturations were also estimated using the closure between cloud droplet number and cloud condensation nuclei (CCN) measurements at various supersaturations (Yum et al., 1998;Sanchez et al., 2016;Sanchez et al., 2021;Saliba et al., 2023).

In summary, direct measurements of water vapor pressure and temperature are essential for quantifying supersaturations; however, they are nearly impossible with current technologies. Supersaturation measurements from aerosol and cloud microphysics monitoring often reflect an effective supersaturation that drives aerosol activation, which is indeed critical in cloud physics. The complexity of cloud formation and evolution and the central role of supersaturation in these processes underscore the need for precise measurement and representation of supersaturation. Advancements in measuring and understanding supersaturation are essential for improving the accuracy of models and reducing uncertainties in weather and climate predictions. In this study, we propose a theoretical framework for using optical methods to observe effective supersaturations based on aerosol activation in clouds and preliminarily validated utilizing data obtained from field campaigns. The feasibility of employing an advanced optical system to measure supersaturation fluctuations were also explored and discussed.

2. Methods and Materials

2.1 Observing effective supersaturations on the basis of κ-Köhler theory

FluctuationsThe concept of effective supersaturation was introduced based on aerosol activation measurements (Hudson and Yum, 1997;Hudson et al., 2010), which could be defined as the supersaturation in CCN chamber (CCN activation under constant supersaturation meanconditions) that resulted in the same aerosol activation fraction with the observed aerosol activation fraction in clouds. Quick fluctuations in supersaturation would result in the effective supersaturation, which directly affectsdetermined by aerosol activation, differs from the mean supersaturation. The which is determined by average water vapor content and temperature. However, the concept of κ-Köhler theory

is established according to a constant supersaturation scenario, therefore provides a framework for deriving effective supersaturation from aerosol activation measurements in clouds (Petters and Kreidenweis, 2007):

$$S = \frac{D^3 - D_d{}^3}{D^3 - D_d{}^3(1-\kappa)} \cdot \exp\left(\frac{4\sigma_{s/a} \cdot M_{water}}{R \cdot T \cdot D_p \cdot g \cdot \rho_w}\right) \qquad (1)$$

where S is the saturation ratio, S-1 represents supersaturation, D is the over an aqueous solution droplet with a diameter of D, D_d is the dry diameter, $\sigma_{s/a}$ is the surface tension of solution/air interface, T is the temperature, M_{water} is the molecular weight of water, R is the universal gas constant, ρ_w is the density of water, and κ is the hygroscopicity parameter. The κ-Köhler theory tells that if the critical diameter of aerosol activation (D_a) and corresponding aerosol hygroscopicity parameter κ are known, the surrounding supersaturation can be retrieved based on air temperature measurements and by assuming $\sigma_{s/a}$ the surface tension of water (as shown in Fig.S1a). Note that D_a and κ are not independent with each other, average κ of aerosols with diameter D_a is needed. Previous studies have shown that the reduction in surface tension (Nozière et al., 2010;Gérard et al., 2016;Ovadnevaite et al., 2017) associated with surfactants in atmospheric aerosols can affect aerosol activation and, consequently, the derivation of effective supersaturation. However, if the derivation of κ (as done in this study) assumes a constant water surface tension, the impact of surface tension changes is minimized, as these effects are already incorporated in the κ calculation. Nonetheless, differences in surface tension between supersaturated and subsaturated conditions (Davies et al., 2019;Petters and Kreidenweis, 2013;Liu et al., 2018), and their impact on effective supersaturation, still exist. Additionally, prior research has suggested that slightly soluble components in aerosols can influence κ values under both supersaturated and subsaturated conditions (Ho et al., 2010;Petters and Kreidenweis, 2008;Lee et al., 2022;Han et al., 2022;Riipinen et al., 2015;Wang et al., 2019;Whitehead et al., 2014). Therefore, κ observed under subsaturated conditions would affect the derivation of effective supersaturation.

However, the simultaneous measurements of D_a and κ of activated aerosols with diameters around D_a are indeed challenging. The direct measurements of size-resolved activation ratio (AR) in clouds are essential for D_a retrievals through the following equation:

$$AR(D_p) = \frac{MAF}{2}\left(1 + \mathrm{erf}\left(\frac{D_p - D_a}{\sqrt{2\pi}\sigma}\right)\right) \qquad (2)$$

178 Where D_p is the particle diameter, MAF is the maximum activation fraction and D_a is critical

179 activation diameter, σ is associated with the slope of the ~~curve near D_a.~~size-resolved AR curve near

180 D_a and mostly influenced by the heterogeneous distribution of aerosols near D_a as well as

181 supersaturation fluctuations (note that not effective supersaturation fluctuations). This formula was

182 previously proposed by Rose et al. (2008) to fit the AR measurements and widely used in AR

183 parameterizations (Tao et al., 2018b). Therefore, it typically requires a unique inlet system and a suite

184 of instruments that measure the aerosol size distribution of both interstitial and total aerosol

185 populations (Hammer et al., 2014;Zíková et al., 2020). Consequently, this is rarely done, even in

186 ground fog measurements. Instead, D_a was usually estimated from aerosol measurements and fog

187 droplet size distributions measurements which indirectly provides the number concentrations of

188 activated aerosols therefore could be used in retrieving D_a through assuming that all aerosols larger

189 than D_a are activated (Mazoyer et al., 2019;Wainwright et al., 2021;Shen et al., 2018) which brings

190 uncertainty in D_a derivations due to that ~~the maximum activation fraction of~~not all aerosols larger than

191 D_a are activated, because the MAF in Eq.2 does not equal to unit although usually very close to (Tao

192 et al., 2018b). For the effective supersaturation measured in aloft clouds, the aerosol number size

193 distributions inside and outside the cloud as well as cloud droplet number concentrations were used by

194 Ditas et al. (2012) to derive D_a, and other approaches were also used (Gong et al., 2023). The κ values

195 were usually retrieved from size-resolved cloud condensation nuclei measurements under certain

196 supersaturations (Hammer et al., 2014;Mazoyer et al., 2019) or from growth factor measurements

197 (Wainwright et al., 2021) or sometime assumed due to the lack of measurements. The κ of activated

198 aerosols were not directly measured in these studies due to the difficulty of the direct sampling of

199 activated aerosols as well as subsequent hygroscopicity measurements.

200   Two types of supersaturation fluctuations have been previously identified. The first type involves

201 fluctuations in supersaturation directly governed by water vapor pressure and temperature, as

202 described by Siebert and Shaw (2017). These fluctuations are linked to turbulence and water phase

203 changes that influence water vapor pressure and temperature. The second type concerns fluctuations

204 in effective supersaturation, which are associated with the activation and deactivation processes of

205 aerosols, as noted by Ditas et al. (2012). The first type of fluctuations dictates the instantaneous growth

206 and evaporation of droplets, thereby controlling the activation and deactivation of cloud droplets. As

207 such, the second type of fluctuation is inherently driven by the first type. The theoretical framework

208 proposed in this study enables the measurement of fluctuations in effective supersaturation.

209

2.2 Field measurements

Kuang et al. [2024] developed an advanced aerosol-cloud sampling system designed to measure fog and cloud activation processes. This compact, integrated system can automatically switch between different inlets, including PM_1 (particles and droplets with an aerodynamic diameter < 1 μm), $PM_{2.5}$ (particles and droplets with an aerodynamic diameter < 2.5 μm) impactor, and Total Suspended Particles (TSP, encompassing all particles and droplets) (as shown in Fig. S2). When combined with instruments that measure aerosol physical, optical, and chemical properties, this system is well-suited for investigating cloud microphysics and chemistry. It was utilized in the AQ-SOFAR campaign, dedicated to studying AQueous Secondary aerOsol formation in Fogs and Aerosols and their Radiative effects in the North China Plain (Kuang et al., 2024).

During this campaign, several radiation fog events were observed, enabling the measurement of size-resolved AR curves, aerosol hygroscopicity as well as chemical compositions of interstitial and activated aerosols within fogs. These measurements provided insights into the evolution of supersaturations (Kuang et al., 2024). Notably, aerosol hygroscopicity was determined using a humidified nephelometer system, located downstream of the inlet system. This system measured multiwavelength scattering coefficients (450 nm, 525 nm, 635 nm) under both nearly dry (RH<20%) and humid conditions (RH~84%), offering aerosol hygroscopicity data based on the optical theory proposed by Kuang et al. (2017). The size-resolved AR curves and aerosol chemical compositions were obtained through the aerosol size distribution and the aerosol mass spectrometry measurements downstream of the inlet system. A schematic of the inlet system and associated instruments is provided in Fig. S1. Further details about the entire experimental setup, size-resolved AR calculations as well as data analysis about mass spectrometer measurements can be found in Kuang et al. (2024).

In addition, the particle number size distributions (PNSDs) in dry state, which range from about 10 nm to 10 μm, were jointly measured by a Twin Differential Mobility Particle Sizer (TDMPS, Leibniz-Institute for Tropospheric Research, Germany) or a scanning mobility particle size spectrometer (SMPS) and an Aerodynamic Particle Sizer (APS, TSI Inc., Model 3321) in six field campaigns conducted on the North China Plain which are detailed in Kuang et al. (2018). The mass concentrations of black carbon (BC) were measured using a Multi-Angle Absorption Photometer (MAAP Model 5012, Thermo, Inc., Waltham, MA USA) or an aethalometer (AE33) (Drinovec et al., 2015) in these field campaigns. Details about these measurements and quality assurance was introduced in Kuang et al. (2018).

2.3 Method of simulating scattering coefficients of interstital aerosols and activated aerosols

For each paired PNSD and BC mass concentration, the size distribution of dry-state PM_1 was obtained using the following formula (the penetration curve shape from Gussman et al. (2002) was also included for considering the non-ideality cutoff of the impactor, and assuming aerosol density of 1.6 g/cm^3 for converting aerodynamic diameter to mobility diameter) :

$$PNSD\ (D_p)_{PM_1} = PNSD\ (D_p) \times R(D_p) \hspace{5cm} (3)$$

Where R(Dp) is the penetration ratio of aerosols as a function of particle diameter D_p of the PM_1 impactor. Further, $PNSD\ (D_p)_{PM_1}$ and the BC mass concentration was used to simulate the size-resolved aerosol scattering coefficients ($d\sigma_{sp}/dlogDp$) at 450 nm, 525 nm and 636 nm that is consistent with the angular truncation and light source nonideality of Auora 3000 nephelometer (Müller et al., 2011), where σ_{sp} represents aerosol scattering coefficient. In this Mie calculation, the shape of black carbon mass size distributions are consistent with the one used in simulations of Kuang et al. (2017) assuming fractions of BC mass that are externally mixed is 0.5. Details about the Mie theory calculations can also be found in Ma et al. (2011) and Kuang et al. (2017).

With given size-resolved AR curve that produced using Eq.2, the size-resolved aerosol scattering coefficients of interstitial aerosols can be calculated using the following formula:

$$d\sigma_{sp,inter}/dlog\mathrm{D_p}\ (D_p) = d\sigma_{sp}/dlog\mathrm{D_p}\ (D_p) \times (1 - AR(D_p)) \hspace{2cm} (4)$$

The size-resolved aerosol scattering coefficients of activated aerosols can be calculated using:

$$d\sigma_{sp,act}/dlog\mathrm{D_p}\ (D_p) = d\sigma_{sp}/dlog\mathrm{D_p}\ (D_p) - d\sigma_{sp,inter}/dlog\mathrm{D_p}\ (D_p) \hspace{1.5cm} (5)$$

Scattering coefficients of total aerosol populations (interstitial plus activated) and interstitial aerosols can be derived through integration of $d\sigma_{sp}/dlog\mathrm{D_p}\ (D_p)$ and $d\sigma_{sp,inter}/dlog\mathrm{D_p}\ (D_p)$.

3. Theoretical Framework and Concept Design of the Advanced Optical System

3.1 Theory of Observing Critical Activation Diameter Using Scattering Measurements

The typical shape of size-resolved AR curves observed in atmospheric fogs and clouds is illustrated in Fig. 1a (Ditas et al., 2012;Hammer et al., 2014;Zíková et al., 2020;Wainwright et al., 2021;Kuang et al., 2024). In clouds, aerosols can be classified as either activated aerosols, which form

299   cloud droplets, or inactivated aerosols, which remain as interstitial aerosols. The critical diameter that

300   distinguishes interstitial aerosols from cloud or fog droplets varies depending on the supersaturation

301   (Kuang et al., 2024). A diameter of 2.5 μm is typically suitable for surface fogs with relatively lower

302   supersaturations (<0.1%), while 1 μm is more appropriate for aloft clouds with higher supersaturations

303   (>0.1%) (Mazoyer et al., 2019;Kuang et al., 2024;Lu et al., 2020). The typical AR curve shows that

304   most aerosols larger than D_a are activated, while most smaller aerosols remain inactivated. As a result,

305   the scattering properties, such as size-resolved scattering coefficients (Fig.1a), the scattering Ångström

306 exponent (SAE) and its wavelength dependence, which are directly related to aerosol size distribution,

307 differ significantly between interstitial and activated aerosols.
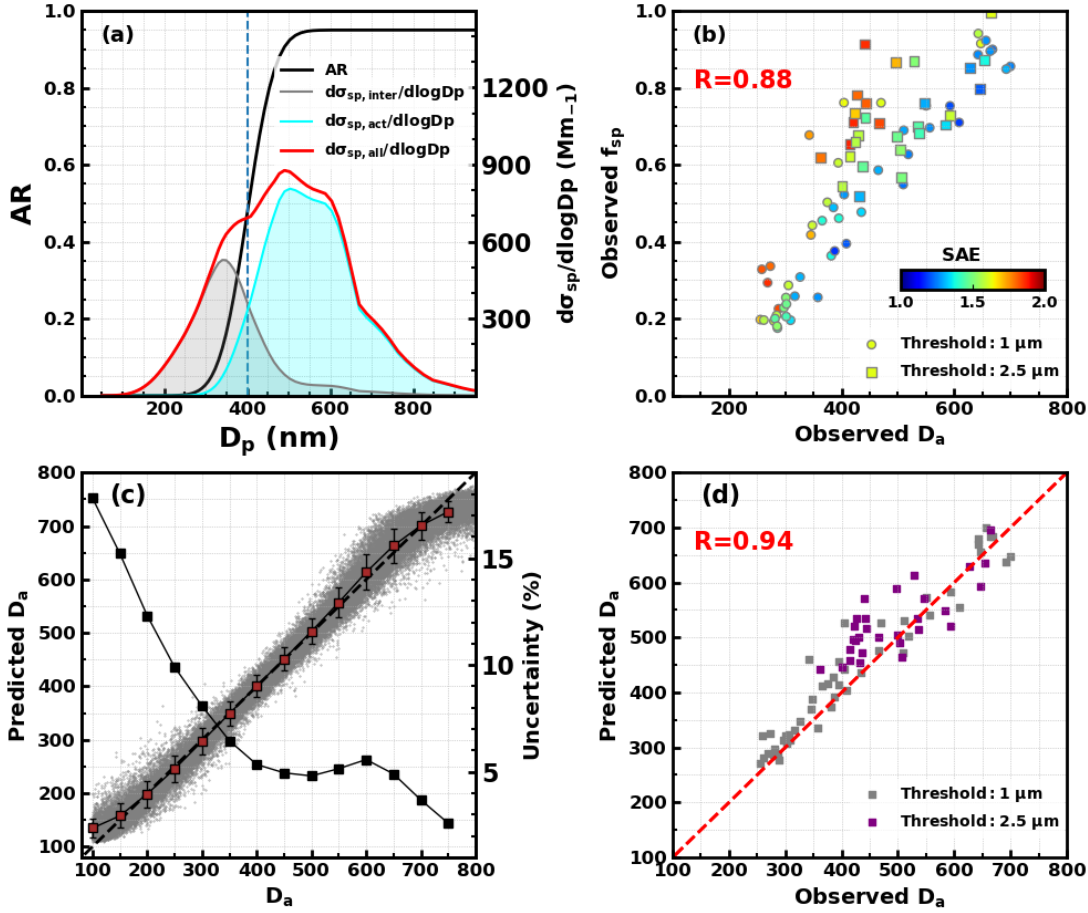
Figure 1. **(a)**The typical shape of size-resolved aerosol activation ratio (AR) curve produced using the function of Eq.2, with the Da of 400 nm, the MAF of 0.95 and the σ of 30, and the average PNSD observed in the North China Plain from six campaigns (Kuang et al., 2018) and the AR curve was used to simulate an example of the size-resolved aerosol scattering ($\sigma_{\overline{sp}}$) distributions of interstitial and activated aerosols at 525 nm; **(b)** Relations between observed $D_{\overline{a}}$ and f_{sp} during the AQ-SOFAR campaign using 1 and 2.5 µm as the threshold of interstital aerosols, with the scatter points are colored with corresponding SAE of total dry state PM₁ aerosols. **(c)** Comparisons of all prescribed $D_{\overline{a}}$ and predicted $D_{\overline{a}}$ values represented by scatter points, they are further binned with interval of 50 nm, averages and standard deviations represented by purple squares and their error bars, black squares represent relative uncertainty of the right axis at each bin; **(d)** The comparisons of $D_{\overline{a}}$ retrieved using activation ratio observations and those predicted using scattering observations as inputs of the trained model, dashed lines represent 1:1 lines.

308 If we focus on PM₁ of the total dry aerosol population (the reasoning for this is discussed in Sect.

309 S1 of the supplement), the scattering fraction of interstitial aerosols in the total dry PM₁ population,

310 defined as $f_{sp} = \sigma_{sp,PM_1,inter}(dry, 525\ nm)/\sigma_{sp,PM_1,all}(dry, 525\ nm)$, where

311 $\sigma_{sp,PM_1,inter}(dry, 525\ nm)$ is the scattering coefficient of PM₁ interstitial aerosols in a dry state at a

312 wavelength of 525 nm, and $\sigma_{sp,PM_1,all}(dry, 525\ nm)$ is that of all PM₁ aerosols, is likely to be highly

313   correlated with D_a. Generally, the larger the D_a, the higher the f_{sp}. This relationship was directly

314   confirmed using D_a and the scattering properties of dry PM_1 interstitial and total aerosols during the

315   AQ-SOFAR campaign, as shown in Fig. 1b, that observed D_a correlates highly with observed f_{sp}

316   (R=0.88). However, at a given D_a, f_{sp} can vary significantly, and these variations are closely related

317   to the SAE of all dry PM_1 aerosols, which are mainly determined by aerosol size distribution. In fact,

318   aside from the size distribution of the total aerosol population that determines SAE, the shape of the

319   AR curve also plays a significant role in the variations of f_{sp}.

320   The nephelometer measures the aerosol scattering coefficient at three wavelengths, enabling

321   direct measurements of the SAE for both the total dry-state PM_1 aerosols and the interstitial aerosols.

322   Therefore, the relationship between f_{sp} and D_a can be further constrained by the SAE of interstitial

323   and activated aerosols, as well as their wavelength dependence. This implies that a simple formulaic

324   relationship between f_{sp} and D_a may not exist. However, the six scattering parameters

325    $\sigma_{sp,PM_1,inter}(dry, \lambda)$—at 450 nm, 525 nm, 635 nm, and $\sigma_{sp,PM_1,all}(dry, \lambda)$ at 450 nm, 525 nm, 635

326   nm—contain both the f_{sp} information and the SAE characteristics of both aerosol groups, thus

327   potentially be used to accurately retrieve D_a. Machine learning techniques, which are well-suited for

328   handling complex relationships, can be applied to this problem.

329   This assumption was tested using Mie theory, based on aerosol size distributions sampled during

330   six campaigns conducted in the North China Plain region (Kuang et al., 2018). For each aerosol size

331   distribution, we randomly assumed different activation curves using Eq.2. ~~The details of this~~

332   ~~simulation are provided in Sect. S2 of the supplement. The simulation pairs of these six scattering~~

333   ~~parameters and D_a were used to train a random forest model (Kuang et al., 2018). To preliminarily~~

334   ~~validate this approach, we randomly selected 75% of the simulated data points for training the model,~~

335   ~~while the remaining 25% were used for validation.~~ That is, for each PNSD from those campaigns, the

336   scattering coefficients of submicron interstitial and activated+interstital aerosols at wavelengths of 450

337   nm, 525 nm and 635 nm corresponding to nephelometer case under 100 size-resolved AR scenarios

338   were simulated using the procedure. And each size-resolved AR curve was produced by using

339   randomly produced D_a, σ and MAF as inputs of Eq.2. In the random step, the range of D_a is 100-700

340   nm, the range of σ is 1-30, the range of MAF is 0.5-1. In each pair, simulated $\sigma_{sp,PM_1,inter}(dry, \lambda)$—

341   at 450 nm, 525 nm, 635 nm, and $\sigma_{sp,PM_1,all}(dry, \lambda)$ at 450 nm, 525 nm, 635 nm was the x values of

342   the random forest model, corresponding D_a is the y value of the random forest model, and the random

343   forest package from Python Scikit–Learn machine learning library (http://scikit-

The results, shown in Fig. 1c, indicate that this approach could retrieve D_a with an uncertainty of less than 10% for D_a larger than 250 nm, and even as low as ~6% for D_a larger than 350 nm. However, the uncertainty increases as D_a decreases, particularly for D_a smaller than 250 nm. The larger uncertainty at smaller D_a is ~~due to the fact that~~since aerosols smaller than 250 nm typically contribute less than 10% to total scattering in the dry state, making f_{sp} less sensitive to variations in D_a. This issue becomes more pronounced when D_a is less than 100 nm, as aerosols smaller than 150 nm generally contribute negligibly to total aerosol scattering [Kuang et al., 2018]. This method was further validated using observations from the AQ-SOFAR campaign. In this validation, D_a values were first predicted using aerosol scattering observations with the trained model and then compared with D_a values retrieved from size-resolved AR measurements, as shown in Fig. 1d. It should be noted that the impactor operates in a sequence of PM$_1$, PM$_{2.5}$, TSP, and then back to PM$_1$, with the flow alternating between a thermodenuder and bypass every 10 minutes for each inlet. To calculate size-resolved AR curves, we assumed that aerosol populations remained unchanged during the 30-minute period (based on comparisons between PM$_1$/PM$_{2.5}$ and TSP inlets), which can sometimes introduce significant uncertainties in the size-resolved AR calculations. When using PM$_{2.5}$ as the threshold, the much lower number concentrations of aerosols larger than 400 nm can introduce more uncertainty in D_a retrievals, partially explaining the lower performance in Fig. 1d when using the PM$_{2.5}$ threshold.

3.2 Method of observing Hygroscopicity of Activated Aerosols

Measuring the hygroscopicity κ of activated aerosols at the critical activation diameter D_a under varying supersaturations is challenging, not only due to technical limitations but also because of the inherent variability in D_a. Kuang et al. (2017) introduced a novel optical method for observing aerosol hygroscopicity by using the aerosol light scattering enhancement factor $f(RH)$ that associated with aerosol hygroscopic growth. This method is particularly suitable for the objectives outlined here. The method requires SAE and light scattering enhancement factors $f(RH)$ of activated aerosols as inputs, and retrieved κ can be termed as $\kappa_{act,f(RH)}$ which represents the overall hygroscopicity of activated aerosols and can be understood as the average κ of activated aerosols with the scattering contribution of each aerosol particle as the weight (Kuang et al., 2020). The scattering coefficients of activated aerosols at multiwavelength can be calculated as $\sigma_{sp,PM_1,act}(dry,\lambda) = \sigma_{sp,PM_1,all}(dry,\lambda) -$

375    $\sigma_{sp,PM_1,inter}(dry,\lambda)$, therefore corresponding SAE can be obtained. The $f(RH)$ of activated aerosols

376   at 525 nm can be calculated as the following:

377    $$f(RH)_{act} = \frac{\sigma_{sp,PM_1,all}\,(RH,525\,nm) - \sigma_{sp,PM_1,inter}(RH,525\,nm)}{\sigma_{sp,PM_1,all}(dry,525\,nm) - \sigma_{sp,PM_1,inter}(dry,525\,nm)} \qquad (6)$$

378   During the AQ-SOFAR campaign, a humidified nephelometer system consisting of two

379   nephelometers—one measuring aerosol scattering in the dry state and the other at a fixed RH of 84%—

380   was placed downstream of the PM_1 impactor. This setup allows for the humidification of dry-state

381   interstitial aerosols and total aerosol populations to a high RH (e.g., above 80%), facilitating the

382   required measurements, therefore severs one choice. The Retrieved $\kappa_{act,f(RH)}$ under different D_a

383   conditions are shown in Fig.2a, demonstrating significant variations in $\kappa_{act,f(RH)}$ and its variations

384   need to constrained. Also, the derived $\kappa_{act,f(RH)}$ are compared those estimated from aerosol chemical

385   compositions measurements ($\kappa_{act,chem}$, details about calculation methods can refer to Kuang et al.

386   (2020)), as shown in Fig.2b and in general agree. Note that the mass spectrometer could not identify
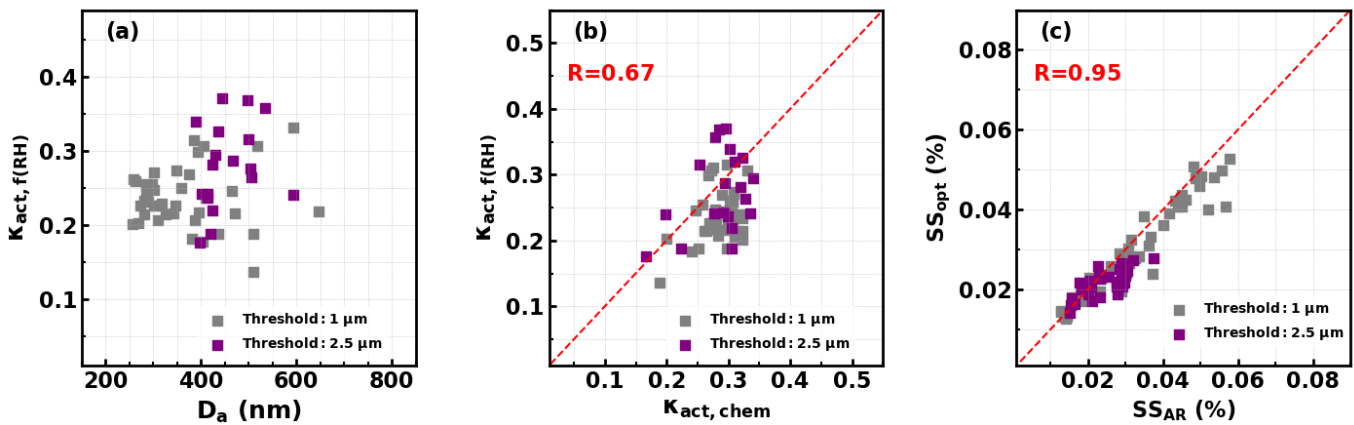
Figure 2. **(a)** Retrieved $\kappa_{act,f(RH)}$ under different D_a conditions; **(b)** Comparison between κ of activated aerosols retrieved from the optical method ($\kappa_{act,f(RH)}$) and estimated from aerosol chemical composition measurements ($\kappa_{act,chem}$) ;**(c)** Comparisons between effective supersaturations (SSs) derived from size-resolved AR measurements as well as $\kappa_{act,chem}$ (SS_{AR}) and from the optical measurements (SS_{opt}). Dashed red lines represent 1:1 lines.

387   all aerosol components, and assumptions about the mixing rule as well as densities of components

388   would bring uncertainties (Kuang et al., 2021). The comparisons between effective supersaturations

389   derived from size-resolved AR measurements as well as $\kappa_{act,chem}$ and from the optical method are

390   shown in Fig.2c. On average, 0.002% of SS bias are observed due to the bias of D_a which associated

391   more with assumptions made in D_a retrievals as previously discussed. As demonstrated by Kuang et

392   al. (2024), for the fog case in the campaign, the threshold of 2.5 μm should be used, however, does not

393   affect the comparisons here.

394 Qiao et al. (2024) developed an advanced outdoor nephelometer system that measures aerosol
395 dry scattering coefficients and scattering coefficients at nearly ambient RH without the need for
396 humidifying the sample air by placing the entire nephelometer system in ambient air, with the
397 instruments protected by a specially designed enclosure. This innovative design offers new insights
398 into the hygroscopicity measurements of activated aerosols. Under cloud conditions, where the
399 ambient RH is close to 100%, aerosol scattering under subsaturated conditions can be measured
400 directly by applying heater.

3.3 Concept Design of the Advanced Optical System for Measuring Effective
401
Supersaturations
402
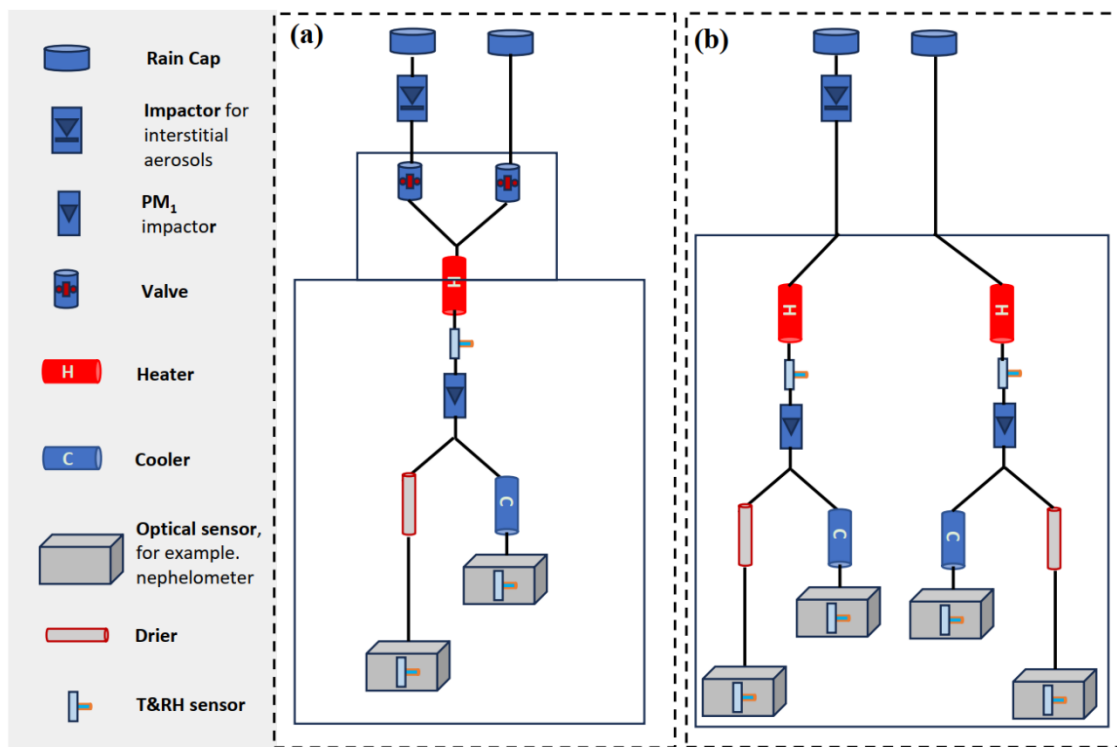
Figure 3. Concept design of the advanced optical system with different number of optical sensors, **(a)** using two nephelometers or other optical sensors; **(b)** using four nephelometers or other optical sensors.

60%, ensuring the evaporation of most of the water content, to make sure the consistency of needed PM_1 cut. The cooler upstream of the 'wet' nephelometer increases the sample RH to approximately 90%, allowing hygroscopicity measurements under conditions close to supersaturation.

403 Based on the proposed optical methods for measuring D_a and $\kappa_{act,f(RH)}$, a conceptual design for
404 outdoor instruments capable of measuring effective supersaturation with relatively high time
405 resolution can be envisioned, as shown in Fig. 3a. The aerosol-cloud sampling system includes two
406 inlets: one equipped with a PM_1 or $PM_{2.5}$ impactor (depending on cloud type) to sample interstitial
407 aerosols, and another with a TSP inlet to sample both interstitial aerosols and cloud/fog droplets. A

408   PM$_1$ impactor is placed downstream of the inlet system, where the RH of the sample air is reduced to

409   70% (as discussed in Sect. S1 of the manuscript) through heater. Downstream of the PM1 impactor,

410   the sample flow is split into two streams: one is further dried to an RH below 10% before aerosol

411   scattering coefficients are measured by the "dry" nephelometer, and the other is passed through an

412   intelligent cooler to ensure the sample RH in the "wet" nephelometer remains close to 90%. The

413   sample air is automatically switched between the interstitial inlet and the TSP inlet at set intervals,

414   such as one minute for each inlet, enabling minute-level measurements of effective supersaturations.

415   While the nephelometer can output scattering measurements every second, reliable data can only be

416   achieved at intervals of around 30 seconds (exact values can be determined through future testing) due

417   to the residence time of aerosols in the nephelometer and potential light source instability. If four

418   nephelometers are available, a more advanced optical system can be designed (Fig. 3b) that does not

419   require switching between the interstitial inlet and the TSP inlet. Instead, two nephelometers would be

420   placed downstream of the interstitial inlet and two downstream of the TSP inlet, enabling higher time

421   resolution effective supersaturation measurements. Other types of optical instruments exist that can

422   achieve stable second-level aerosol scattering or extinction measurements with a stable laser light

423   source [Moise et al., 2015; Zhou et al., 2020]. Therefore, with the development of suitable optical

424   instruments, it may be possible to achieve second-level effective supersaturation measurements.

425   4. Discussions on Limitations and Advantages

426   The proposed theoretical framework enables simultaneous measurements of D_a and κ for

427   activated aerosols, leveraging the high time resolution of optical instruments to potentially provide

428   second-level measurements of supersaturation. However, several limitations should be discussed and

429   might be improved upon: **(1) Shape of size-resolved AR curve:** Cloud chamber studies have shown

430   that supersaturation fluctuations can lead to the coexistence of particles with the same critical

431   supersaturation as both interstitial aerosols and cloud droplets (Shawon et al., 2021). This results in

432   size-resolved AR curves deviate more from stepwise shape, a phenomenon also observed in some field

433   measurements (Henning et al., 2004;Mertes et al., 2007). Despite this, a critical diameter D_a still exists,

434   and such non-ideal curves can be treated a high standard deviation σ in the activation error function

435   (Eq. 2), which does not fundamentally undermine the proposed framework, however, should be further

436   checked for different cloud types. **(2) Measurement of κ:** Although the framework measures the

437   overall κ of activated aerosols, the κ needed for supersaturation calculations is that of aerosols near

438   D_a (κ_{D_a}). For $D_a > \sim 200$ nm, the derived $\kappa_{act,f(RH)}$ can provide a first-order estimate of κ_{D_a}, based on

observed size-dependent characteristics of κ values (Liu et al., 2014;Shen et al., 2021;Wang et al., 2024), though more comprehensive evaluations are needed. Additionally, κ measured under subsaturated conditions differs from that under supersaturated conditions (Tao et al., 2023) might also bring some uncertainties. However, as shown in Fig. S1b, even a bias of 0.1 in κ only ~~results~~result in a ~0.01% bias when SS is ~0.1% and a ~0.005% bias when SS is ~0.05% in supersaturation retrievals, making the first-order estimates of κ_{D_a} from optical measurements generally suitable for supersaturation observations. **(3) Limitations in D_a Retrievals:** Current techniques using aerosol scattering measurements at visible wavelengths (e.g., nephelometers) are reliable only for $D_a>100$ nm as shown in Fig.1a, limiting effective supersaturation measurements to less than 0.21% (assuming a typical κ of 0.3). This restriction makes the technique most applicable to fog and stratus or stratocumulus cloud measurements. However, incorporating scattering measurements at ultraviolet wavelengths could improve sensitivity to smaller D_a and lower κ, enabling measurements in conditions with higher effective supersaturation and a broader range of cloud types in the future.

The uncertainty in effective supersaturation observations using this framework primarily arises from the uncertainties in deriving D_a and κ_{D_a}. The uncertainty in D_a observations using the Aurora 3000 nephelometer as the optical sensor under varying conditions is detailed in Fig. 1c. Factors affecting the accuracy of κ_{D_a} include: (1) the size dependence of κ of activated aerosols; (2) uncertainties related to surface tension, slightly soluble components, and other factors that lead to differences in κ differences under subsaturated and supersaturated conditions. Based on previous studies on the size dependence of κ (Peng et al., 2020) and the differences between subsaturated and supersaturated conditions (Whitehead et al., 2014;Liu et al., 2018;Tao et al., 2023), a 50% uncertainty (three times the standard deviation) was assumed in the derivation of κ_{D_a} for the uncertainty analysis. Using this approach, the uncertainty in effective supersaturation measurements, estimated through the Monte Carlo method, is shown in Fig. 4. The analysis indicates that applying this framework with the Aurora 3000 nephelometer as the optical sensor results in an uncertainty of approximately 5%. The precision of effective supersaturation measurements is directly linked to the accuracy of the optical sensor's scattering signal. For example, the Aurora 3000 has an accuracy of 1 Mm^{-1}, which leads to different levels of precision in D_a and hygroscopicity measurements depending on the scattering signal strength. If the scattering signal from the total aerosol population is 100 Mm^{-1}, the precision of the observed interstitial aerosol scattering fraction f_{sp} is about 1%. Based on the relationship between f_{sp} and D_a shown in Fig. 1b, this leads to a precision of approximately 3 nm for D_a, which results in an effective supersaturation precision of ~0.01% when supersaturation is near 0.2%, or ~0.0002% when

supersaturation is near 0.02%. However, if the scattering signal is lower (e.g., 10 Mm^{-1}), a bias of 1 Mm^{-1} could result in effective supersaturation bias to as much as ~0.07% when supersaturation is near
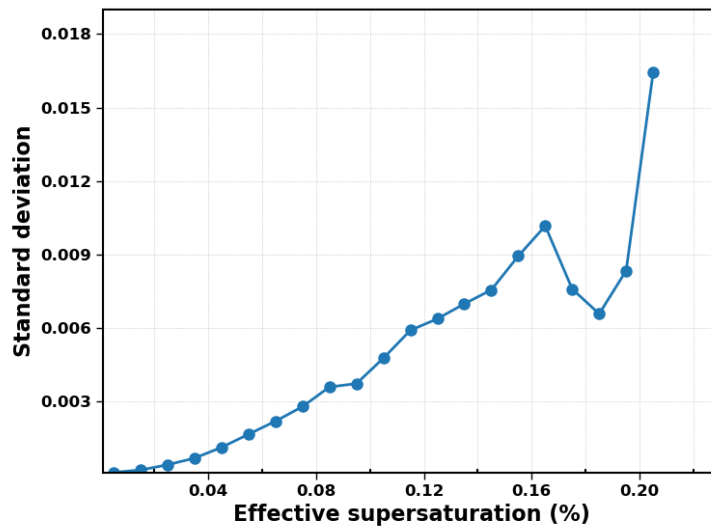
Figure 4. The standard deviations of effective supersaturations under different effective supersaturation (SS) levels.

0.2%, making the measurements unreliable. In summary, while the proposed framework demonstrates the feasibility of observing effective supersaturation with an advanced optical system, the accuracy and precision depend on the resolution of the optical sensors, the scattering parameters being measured, and the scattering signal levels of aerosols in clouds. Enhancing the sensor precision to 0.1 Mm^{-1} or even 0.01 Mm^{-1}, and incorporating ultraviolet wavelengths and multiple scattering angles, might enable high-accuracy supersaturation measurements across a broad range of supersaturation conditions, especially in cleaner environments.

As mentioned in Sect. 2.1, the theoretical framework proposed in this study is designed to observe effective supersaturation fluctuations, rather than supersaturation fluctuations themselves. While there are non-negligible uncertainties associated with observing effective supersaturation using the proposed theory, the size and hygroscopicity distributions of total interstitial and activated aerosol populations remain nearly constant when measured with second-scale or shorter time resolution. The parameter that changes over time is the dynamic exchange between interstitial and activated aerosols. Consequently, fluctuations in the scattering signals of interstitial and activated aerosols can reflect this exchange at high temporal resolution. Since effective supersaturation fluctuations result from underlying supersaturation variations, they could, in principle, provide insights into the causes of these fluctuations, such as turbulence, though this would require further investigation and endeavor. In addition, for size-resolved AR, both σ and MAF are crucial parameters. However, using scattering coefficients at just three wavelengths of Aurora 3000 nephelometer is insufficient for accurately

retrieving σ and MAF. If σ and MAF could be measured more precisely through the extended optical framework, it would provide deeper insights into supersaturation fluctuations.

Despite these limitations, the proposed theoretical framework represents the first system capable of directly providing high time resolution measurements of effective supersaturations using a single instrument. This system is particularly well-suited for surface fog and mountain cloud observations, and when coupled with aerial vehicles, it could also be employed for measurements in aloft clouds. The system offers several advantages for cloud and fog measurements: **(1) High-Resolution Supersaturation Measurements:** The system can provide measurements of effective supersaturations at even a second-level resolution, making it feasible for observing effective supersaturation fluctuations and supporting investigations into fog and cloud evolution mechanisms. **(2) Long-Term Measurement Capability:** The optical measurements, such as those from the nephelometer system, are well-suited for long-term observations, making it possible to acquire climatological data on the variability of fogs and mountain clouds. **(3) Comprehensive Aerosol and Cloud Data:** In addition to measuring effective supersaturations, the system directly captures the scattering and hygroscopic properties of both interstitial and activated aerosols. With further algorithm development, it could also retrieve the number concentrations of available cloud condensation nuclei (CCN) at certain supersaturations, as well as cloud droplet number concentrations, based on previous studies that have observed CCN using optical methods (Tao et al., 2018a). **(4) Monitoring Aerosol Hygroscopic Behavior:** The system continuously monitors aerosol hygroscopic behavior under subsaturated conditions along with the corresponding optical properties. This allows for clear documentation of the formation and dissipation of fog/cloud events, as well as the variation in aerosol optical and hygroscopic properties. Overall, the datasets generated by this system are well-suited for in-depth investigations of cloud physics and aerosol-cloud interactions. This system has the potential to significantly advance fundamental research on clouds and fogs. However, further theoretical studies are needed to refine and optimize this type of system.

521

522

Financial Supports. This work is supported by National Natural Science Foundation of China (42175083, 42175127), and the Fundamental Research Funds for the Central Universities.

525

526 **Competing interests**. The authors declare that they have no conflict of interest.

527

528 **Data Availability**. All data presented in Figures of this manuscript are freely available at Kuang, Y.
529 (2024), and more specific data will be made available on request.

530

531 **Author contribution**. YK conceived the theoretical framework and wrote the manuscript. JT, HX, L
532 L, WX and WeX participated the field campaign and conducted measurements of aerosol chemical
533 and physical properties. YS, PL, CZ reviewed and commented on the paper.

534

535

536

537

538

539

540

541

542

543

544

545

546

588

589

590

References

Abade, G. C., Grabowski, W. W., and Pawlowska, H.: Broadening of Cloud Droplet Spectra through Eddy Hopping: Turbulent Entraining Parcel Simulations, Journal of the Atmospheric Sciences, 75, 3365-3379, https://doi.org/10.1175/JAS-D-18-0078.1, 2018.

Abdul-Razzak, H., Ghan, S. J., and Rivera-Carpio, C.: A parameterization of aerosol activation: 1. Single aerosol type, Journal of Geophysical Research: Atmospheres, 103, 6123-6131, https://doi.org/10.1029/97JD03735, 1998.

Anderson, J. C., Beeler, P., Ovchinnikov, M., Cantrell, W., Krueger, S., Shaw, R. A., Yang, F., and Fierce, L.: Enhancements in Cloud Condensation Nuclei Activity From Turbulent Fluctuations in Supersaturation, Geophysical Research Letters, 50, e2022GL102635, https://doi.org/10.1029/2022GL102635, 2023.

Chandrakar, K. K., Cantrell, W., Chang, K., Ciochetto, D., Niedermeier, D., Ovchinnikov, M., Shaw, R. A., and Yang, F.: Aerosol indirect effect from turbulence-induced broadening of cloud-droplet size distributions, Proceedings of the National Academy of Sciences, 113, 14243-14248, doi:10.1073/pnas.1612686113, 2016.

Chandrakar, K. K., Cantrell, W., and Shaw, R. A.: Influence of Turbulent Fluctuations on Cloud Droplet Size Dispersion and Aerosol Indirect Effects, Journal of the Atmospheric Sciences, 75, 3191-3209, https://doi.org/10.1175/JAS-D-18-0006.1, 2018.

Chandrakar, K. K., Saito, I., Yang, F., Cantrell, W., Gotoh, T., and Shaw, R. A.: Droplet size distributions in turbulent clouds: experimental evaluation of theoretical distributions, Quarterly Journal of the Royal Meteorological Society, 146, 483-504, https://doi.org/10.1002/qj.3692, 2020.

Cooper, W. A.: Effects of Variable Droplet Growth Histories on Droplet Size Distributions. Part I: Theory, Journal of Atmospheric Sciences, 46, 1301-1311, https://doi.org/10.1175/1520-0469(1989)046<1301:EOVDGH>2.0.CO;2, 1989.

Davies, J. F., Zuend, A., and Wilson, K. R.: Technical note: The role of evolving surface tension in the formation of cloud droplets, Atmospheric Chemistry and Physics, 19, 2933-2946, 10.5194/acp-19-2933-2019, 2019.

Ditas, F., Shaw, R. A., Siebert, H., Simmel, M., Wehner, B., and Wiedensohler, A.: Aerosols-cloud microphysics-thermodynamics-turbulence: evaluating supersaturation in a marine stratocumulus cloud, ~~Atmos. Chem. Phys.,~~ Atmospheric Chemistry and Physics, 12, 2459-2468, 10.5194/acp-12-2459-2012, 2012.

Gérard, V., Nozière, B., Baduel, C., Fine, L., Frossard, A. A., and Cohen, R. C.: Anionic, Cationic, and Nonionic Surfactants in Atmospheric Aerosols from the Baltic Coast at Askö, Sweden: Implications for Cloud Droplet Activation, Environmental science & technology, 50, 2974-2982, 10.1021/acs.est.5b05809, 2016.

Gong, X., Wang, Y., Xie, H., Zhang, J., Lu, Z., Wood, R., Stratmann, F., Wex, H., Liu, X., and Wang, J.: Maximum Supersaturation in the Marine Boundary Layer Clouds Over the North Atlantic, AGU Advances, 4, e2022AV000855, https://doi.org/10.1029/2022AV000855, 2023.

Gussman, R. A., Kenny, L. C., Labickas, M., and Norton, P.: Design, Calibration, and Field Test of a Cyclone for PM 1 Ambient Air Sampling, Aerosol Science and Technology, 36, 361-365, 10.1080/027868202753504461, 2002.

Hammer, E., Gysel, M., Roberts, G. C., Elias, T., Hofer, J., Hoyle, C. R., Bukowiecki, N., Dupont, J. C., Burnet, F., Baltensperger, U., and Weingartner, E.: Size-dependent particle activation properties in fog during the ParisFog 2012/13 field campaign, Atmos. Chem. Phys.,Atmospheric Chemistry and Physics, 14, 10517-10533, 10.5194/acp-14-10517-2014, 2014.

Han, S., Hong, J., Luo, Q., Xu, H., Tan, H., Wang, Q., Tao, J., Zhou, Y., Peng, L., He, Y., Shi, J., Ma, N., Cheng, Y., and Su, H.: Hygroscopicity of organic compounds as a function of organic functionality, water solubility, molecular weight, and oxidation level,Atmospheric Chemistry and Physics., 22, 3985-4004, 10.5194/acp-22-3985-2022, 2022.

Henning, S., Bojinski, S., Diehl, K., Ghan, S., Nyeki, S., Weingartner, E., Wurzler, S., and Baltensperger, U.: Aerosol partitioning in natural mixed-phase clouds, Geophysical Research Letters, 31, https://doi.org/10.1029/2003GL019025, 2004.

Ho, K. F., Lee, S. C., Ho, S. S. H., Kawamura, K., Tachibana, E., Cheng, Y., and Zhu, T.: Dicarboxylic acids, ketocarboxylic acids, α-dicarbonyls, fatty acids, and benzoic acid in urban aerosols collected during the 2006 Campaign of Air Quality Research in Beijing (CAREBeijing-2006), Journal of Geophysical Research: Atmospheres, 115, https://doi.org/10.1029/2009JD013304, 2010.

Hudson, J. G., and Yum, S. S.: Droplet Spectral Broadening in Marine Stratus, Journal of the Atmospheric Sciences, 54, 2642-2654, https://doi.org/10.1175/1520-0469(1997)054<2642:DSBIMS>2.0.CO;2, 1997.

Hudson, J. G., Noble, S., and Jha, V.: Stratus cloud supersaturations, Geophysical Research Letters, 37, https://doi.org/10.1029/2010GL045197, 2010.

Kaufman, Y. J., and Tanré, D.: Effect of variations in super-saturation on the formation of cloud condensation nuclei, Nature, 369, 45-48, 10.1038/369045a0, 1994.

Kuang, Y., Zhao, C., Tao, J., Bian, Y., Ma, N., and Zhao, G.: A novel method for deriving the aerosol hygroscopicity parameter based only on measurements from a humidified nephelometer system, Atmos. Chem. Phys.,Atmospheric Chemistry and Physics, 17, 6651-6662, 10.5194/acp-17-6651-2017, 2017.

Kuang, Y., Zhao, C. S., Zhao, G., Tao, J. C., Xu, W., Ma, N., and Bian, Y. X.: A novel method for calculating ambient aerosol liquid water content based on measurements of a humidified nephelometer system, Atmospheric Measurement Techniques, 11, 2967-2982, 10.5194/amt-11-2967-2018, 2018.

Kuang, Y., He, Y., Xu, W., Zhao, P., Cheng, Y., Zhao, G., Tao, J., Ma, N., Su, H., Zhang, Y., Sun, J., Cheng, P., Yang, W., Zhang, S., Wu, C., Sun, Y., and Zhao, C.: Distinct diurnal variation in organic aerosol hygroscopicity and its relationship with oxygenated organic aerosol, Atmos. Chem. Phys.,Atmospheric Chemistry and Physics, 20, 865-880, 10.5194/acp-20-865-2020, 2020.

Kuang, Y., Huang, S., Xue, B., Luo, B., Song, Q., Chen, W., Hu, W., Li, W., Zhao, P., Cai, M., Peng, Y., Qi, J., Li, T., Wang, S., Chen, D., Yue, D., Yuan, B., and Shao, M.: Contrasting effects of secondary organic aerosol formations on organic aerosol hygroscopicity, Atmos. Chem. PhysAtmospheric Chemistry and Physics., 21, 10375-10391, 10.5194/acp-21-10375-2021, 2021.

Kuang, Y., Xu, W., Tao, J., Luo, B., Liu, L., Xu, H., Xu, W., Xue, B., Zhai, M., Liu, P., and Sun, Y.: Divergent Impacts of Biomass Burning and Fossil Fuel Combustion Aerosols on Fog-Cloud Microphysics and Chemistry: Novel Insights From Advanced Aerosol-Fog Sampling, Geophysical Research Letters, 51, e2023GL107147, https://doi.org/10.1029/2023GL107147, 2024.

Lee, W.-C., Deng, Y., Zhou, R., Itoh, M., Mochida, M., and Kuwata, M.: Water Solubility Distribution of Organic Matter Accounts for the Discrepancy in Hygroscopicity among Sub- and Supersaturated Humidity Regimes, Environmental science & technology, 10.1021/acs.est.2c04647, 2022.

Liu, H. J., Zhao, C. S., Nekat, B., Ma, N., Wiedensohler, A., van Pinxteren, D., Spindler, G., Müller, K., and Herrmann, H.: Aerosol hygroscopicity derived from size-segregated chemical composition and its parameterization in the North China Plain, ~~Atmos. Chem. Phys.,~~ Atmospheric Chemistry and Physics, 14, 2525-2539, 10.5194/acp-14-2525-2014, 2014.

Liu, P., Song, M., Zhao, T., Gunthe, S. S., Ham, S., He, Y., Qin, Y. M., Gong, Z., Amorim, J. C., Bertram, A. K., and Martin, S. T.: Resolving the mechanisms of hygroscopic growth and cloud condensation nuclei activity for organic particulate matter, Nature communications, 9, 4076, 10.1038/s41467-018-06622-2, 2018.

Lu, C., Liu, Y., Yum, S. S., Chen, J., Zhu, L., Gao, S., Yin, Y., Jia, X., and Wang, Y.: Reconciling Contrasting Relationships Between Relative Dispersion and Volume-Mean Radius of Cloud Droplet Size Distributions, Journal of Geophysical Research: Atmospheres, 125, e2019JD031868, https://doi.org/10.1029/2019JD031868, 2020.

Müller, T., Laborde, M., Kassell, G., and Wiedensohler, A.: Design and performance of a three-wavelength LED-based total scatter and backscatter integrating nephelometer, Atmospheric Measurement Techniques, 4, 1291-1303, 10.5194/amt-4-1291-2011, 2011.

Ma, N., Zhao, C. S., Nowak, A., Müller, T., Pfeifer, S., Cheng, Y. F., Deng, Z. Z., Liu, P. F., Xu, W. Y., Ran, L., Yan, P., Göbel, T., Hallbauer, E., Mildenberger, K., Henning, S., Yu, J., Chen, L. L., Zhou, X. J., Stratmann, F., and Wiedensohler, A.: Aerosol optical properties in the North China Plain during HaChi campaign: an in-situ optical closure study, Atmospheric Chemistry and Physics, 11, 5959-5973, 10.5194/acp-11-5959-2011, 2011.

Mazoyer, M., Burnet, F., Denjean, C., Roberts, G. C., Haeffelin, M., Dupont, J. C., and Elias, T.: Experimental study of the aerosol impact on fog microphysics, ~~Atmos. Chem. Phys.,~~ Atmospheric Chemistry and Physics, 19, 4323-4344, 10.5194/acp-19-4323-2019, 2019.

Mertes, S., Verheggen, B., Walter, S., Connolly, P., Ebert, M., Schneider, J., Bower, K. N., Cozic, J., Weinbruch, S., Baltensperger, U., and Weingartner, E.: Counterflow Virtual Impactor Based Collection of Small Ice Particles in Mixed-Phase Clouds for the Physico-Chemical Characterization of Tropospheric Ice Nuclei: Sampler Description and First Case Study, Aerosol Science and Technology, 41, 848-864, 10.1080/02786820701501881, 2007.

Nozière, B., Ekström, S., Alsberg, T., and Holmström, S.: Radical-initiated formation of organosulfates and surfactants in atmospheric aerosols, Geophysical Research Letters, 37, https://doi.org/10.1029/2009GL041683, 2010.

Ovadnevaite, J., Zuend, A., Laaksonen, A., Sanchez, K. J., Roberts, G., Ceburnis, D., Decesari, S., Rinaldi, M., Hodas, N., Facchini, M. C., Seinfeld, J. H., and C, O. D.: Surface tension prevails over solute effect in organic-influenced cloud droplet activation, Nature, 546, 637-641, 10.1038/nature22806, 2017.

Peng, C., Wang, Y., Wu, Z., Chen, L., Huang, R.-J., Wang, W., Wang, Z., Hu, W., Zhang, G., Ge, M., Hu, M., Wang, X., and Tang, M.: Tropospheric aerosol hygroscopicity in China, Atmospheric Chemistry and Physics, 20, 13877-13903, 10.5194/acp-20-13877-2020, 2020.

Petters, M. D., and Kreidenweis, S. M.: A single parameter representation of hygroscopic growth and cloud condensation nucleus activity, Atmospheric Chemistry and Physics, 7, 1961-1971, 2007.

Petters, M. D., and Kreidenweis, S. M.: A single parameter representation of hygroscopic growth and cloud condensation nucleus activity - Part 2: Including solubility, Atmospheric Chemistry and Physics, 8, 6273-6279, 2008.

Petters, M. D., and Kreidenweis, S. M.: A single parameter representation of hygroscopic growth and cloud condensation nucleus activity - Part 3: Including surfactant partitioning, Atmospheric Chemistry and Physics, 13, 1081-1091, 10.5194/acp-13-1081-2013, 2013.

Prabhakaran, P., Shawon, A. S. M., Kinney, G., Thomas, S., Cantrell, W., and Shaw, R. A.: The role of turbulent fluctuations in aerosol activation and cloud formation, Proceedings of the National Academy of Sciences, 117, 16831-16838, 10.1073/pnas.2006426117, 2020.

Qiao, H., Kuang, Y., Yuan, F., Liu, L., Zhai, M., Xu, H., Zou, Y., Deng, T., and Deng, X.: Unlocking the Mystery of Aerosol Phase Transitions Governed by Relative Humidity History Through an Advanced Outdoor Nephelometer System, Geophysical Research Letters, 51, e2023GL107179, https://doi.org/10.1029/2023GL107179, 2024.

Riipinen, I., Rastak, N., and Pandis, S. N.: Connecting the solubility and CCN activation of complex organic aerosols: a theoretical study using solubility distributions, Atmospheric Chemistry and Physics, 15, 6305-6322, 10.5194/acp-15-6305-2015, 2015.

Rose, D., Gunthe, S. S., Mikhailov, E., Frank, G. P., Dusek, U., Andreae, M. O., and Pöschl, U.: Calibration and measurement uncertainties of a continuous-flow cloud condensation nuclei counter (DMT-CCNC): CCN activation of ammonium sulfate and sodium chloride aerosol particles in theory and experiment, ~~Atmos. Chem. Phys.,~~ Atmospheric Chemistry and Physics, 8, 1153-1179, 10.5194/acp-8-1153-2008, 2008.

Saito, I., Gotoh, T., and Watanabe, T.: Broadening of Cloud Droplet Size Distributions by Condensation in Turbulence, Journal of the Meteorological Society of Japan. Ser. II, 97, 867-891, 10.2151/jmsj.2019-049, 2019.

Saliba, G., Bell, D. M., Suski, K. J., Fast, J. D., Imre, D., Kulkarni, G., Mei, F., Mülmenstädt, J. H., Pekour, M., Shilling, J. E., Tomlinson, J., Varble, A. C., Wang, J., Thornton, J. A., and Zelenyuk, A.: Aircraft measurements of single particle size and composition reveal aerosol size and mixing state dictate their activation into cloud droplets, Environmental Science: Atmospheres, 3, 1352-1364, 10.1039/D3EA00052D, 2023.

Sanchez, K. J., Russell, L. M., Modini, R. L., Frossard, A. A., Ahlm, L., Corrigan, C. E., Roberts, G. C., Hawkins, L. N., Schroder, J. C., Bertram, A. K., Zhao, R., Lee, A. K. Y., Lin, J. J., Nenes, A., Wang, Z., Wonaschütz, A., Sorooshian, A., Noone, K. J., Jonsson, H., Toom, D., Macdonald, A. M., Leaitch, W. R., and Seinfeld, J. H.: Meteorological and aerosol effects on marine cloud microphysical properties, Journal of Geophysical Research: Atmospheres, 121, 4142-4161, https://doi.org/10.1002/2015JD024595, 2016.

Sanchez, K. J., Roberts, G. C., Saliba, G., Russell, L. M., Twohy, C., Reeves, J. M., Humphries, R. S., Keywood, M. D., Ward, J. P., and McRobert, I. M.: Measurement report: Cloud processes and the transport of biological emissions affect southern ocean particle and cloud condensation nuclei concentrations, ~~Atmos. Chem. Phys.,~~ Atmospheric Chemistry and Physics, 21, 3427-3446, 10.5194/acp-21-3427-2021, 2021.

Sardina, G., Picano, F., Brandt, L., and Caballero, R.: Continuous Growth of Droplet Size Variance due to Condensation in Turbulent Clouds, Physical Review Letters, 115, 184501, 10.1103/PhysRevLett.115.184501, 2015.

Seinfeld, J., and Pandis, S.: Atmospheric Chemistry and Physics: From Air Pollution to Climate Change, Third Edition, 2016.

Seinfeld, J. H., Bretherton, C., Carslaw, K. S., Coe, H., DeMott, P. J., Dunlea, E. J., Feingold, G., Ghan, S., Guenther, A. B., Kahn, R., Kraucunas, I., Kreidenweis, S. M., Molina, M. J., Nenes, A., Penner, J. E., Prather, K. A., Ramanathan, V., Ramaswamy, V., Rasch, P. J., Ravishankara, A. R., Rosenfeld, D., Stephens, G., and Wood, R.: Improving our fundamental understanding of the role of aerosol−cloud interactions in the climate system, Proceedings of the National Academy of Sciences, 113, 5781-5790, 10.1073/pnas.1514043113, 2016.

Shaw, R. A., Cantrell, W., Chen, S., Chuang, P., Donahue, N., Feingold, G., Kollias, P., Korolev, A., Kreidenweis, S., Krueger, S., Mellado, J. P., Niedermeier, D., and Xue, L.: Cloud–Aerosol–Turbulence Interactions: Science Priorities and Concepts for a Large-Scale Laboratory Facility, Bulletin of the American Meteorological Society, 101, E1026-E1035, https://doi.org/10.1175/BAMS-D-20-0009.1, 2020.

Shawon, A. S. M., Prabhakaran, P., Kinney, G., Shaw, R. A., and Cantrell, W.: Dependence of Aerosol-Droplet Partitioning on Turbulence in a Laboratory Cloud, Journal of Geophysical Research: Atmospheres, 126, e2020JD033799, https://doi.org/10.1029/2020JD033799, 2021.

Shen, C., Zhao, C., Ma, N., Tao, J., Zhao, G., Yu, Y., and Kuang, Y.: Method to Estimate Water Vapor Supersaturation in the Ambient Activation Process Using Aerosol and Droplet Measurement Data, Journal of Geophysical Research: Atmospheres, 0, 10.1029/2018JD028315, 2018.

Shen, C., Zhao, G., Zhao, W., Tian, P., and Zhao, C.: Measurement report: aerosol hygroscopic properties extended to 600 nm in the urban environment, ~~Atmos. Chem. Phys.,~~ Atmospheric Chemistry and Physics, 21, 1375-1388, 10.5194/acp-21-1375-2021, 2021.

Siebert, H., and Shaw, R. A.: Supersaturation Fluctuations during the Early Stage of Cumulus Formation, Journal of the Atmospheric Sciences, 74, 975-988, https://doi.org/10.1175/JAS-D-16-0115.1, 2017.

Tao, J., Zhao, C., Kuang, Y., Zhao, G., Shen, C., Yu, Y., Bian, Y., and Xu, W.: A new method for calculating number concentrations of cloud condensation nuclei based on measurements of a three-wavelength humidified nephelometer system, ~~Atmos. Meas. Tech.,~~ Atmospheric Measurement Techniques, 11, 895-906, 10.5194/amt-11-895-2018, 2018a.

Tao, J., Zhao, C., Ma, N., and Kuang, Y.: Consistency and applicability of parameterization schemes for the size-resolved aerosol activation ratio based on field measurements in the North China Plain, Atmospheric Environment, 173, 316-324, https://doi.org/10.1016/j.atmosenv.2017.11.021, 2018b.

Tao, J., Kuang, Y., Luo, B., Liu, L., Xu, H., Ma, N., Liu, P., Xue, B., Zhai, M., Xu, W., Xu, W., and Sun, Y.: Kinetic Limitations Affect Cloud Condensation Nuclei Activity Measurements Under Low Supersaturation, Geophysical Research Letters, 50, e2022GL101603, https://doi.org/10.1029/2022GL101603, 2023.

Wainwright, C., Chang, R. Y.-W., and Richter, D.: Aerosol Activation in Radiation Fog at the Atmospheric Radiation Program Southern Great Plains Site, Journal of Geophysical Research: Atmospheres, 126, e2021JD035358, https://doi.org/10.1029/2021JD035358, 2021.

Wang, J., Shilling, J. E., Liu, J., Zelenyuk, A., Bell, D. M., Petters, M. D., Thalman, R., Mei, F., Zaveri, R. A., and Zheng, G.: Cloud droplet activation of secondary organic aerosol is mainly controlled by molecular weight, not water solubility, Atmospheric Chemistry and Physics, 19, 941-954, 10.5194/acp-19-941-2019, 2019.

Wang, Y., Li, J., Fang, F., Zhang, P., He, J., Pöhlker, M. L., Henning, S., Tang, C., Jia, H., Wang, Y., Jian, B., Shi, J., and Huang, J.: In-situ observations reveal weak hygroscopicity in the Southern Tibetan Plateau: implications for aerosol activation and indirect effects, npj Climate and Atmospheric Science, 7, 77, 10.1038/s41612-024-00629-x, 2024.

Whitehead, J. D., Irwin, M., Allan, J. D., Good, N., and McFiggans, G.: A meta-analysis of particle water uptake reconciliation studies, Atmospheric Chemistry and Physics, 14, 11833-11841, 10.5194/acp-14-11833-2014, 2014.

Yang, F., McGraw, R., Luke, E. P., Zhang, D., Kollias, P., and Vogelmann, A. M.: A new approach to estimate supersaturation fluctuations in stratocumulus cloud using ground-based remote-sensing measurements, ~~Atmos. Meas. Tech.,~~Atmospheric Measurement Techniques, 12, 5817-5828, 10.5194/amt-12-5817-2019, 2019.

Yum, S. S., Hudson, J. G., and Xie, Y.: Comparisons of cloud microphysics with cloud condensation nuclei spectra over the summertime Southern Ocean, Journal of Geophysical Research: Atmospheres, 103, 16625-16636, https://doi.org/10.1029/98JD01513, 1998.

Zíková, N., Pokorná, P., Makeš, O., Sedlák, P., Pešice, P., and Ždímal, V.: Activation of atmospheric aerosols in fog and low clouds, Atmospheric Environment, 230, 117490, https://doi.org/10.1016/j.atmosenv.2020.117490, 2020.

带格